Analysis of free-surface flows through energy considerations: single-phase vs two-phase modeling

Salvatore Marrone

CNR-INSEAN, Marine Technology Research Institute,

Rome, Italy and

École Centrale Nantes,

LHEEA Lab.(ECN / CNRS), Nantes, France

Andrea Colagrossi*

CNR-INSEAN, Marine Technology Research Institute, Rome, Italy

Andrea Di Mascio

CNR IAC, Istituto per le Applicazioni del Calcolo "Mauro Picone", Rome, Italy

David Le Touzé

École Centrale Nantes,

LHEEA Lab. (ECN / CNRS), Nantes, France

(Dated: May 17, 2016)

Abstract

The study of energetic free-surface flows is challenging because of the large range of interface scales involved due to multiple fragmentations and reconnections of the air-water interface, with formation of drops and bubbles. Because of their complexity the investigation of such phenomena through numerical simulation largely increased during the recent years. Actually, in the last decades different numerical models have been developed to study these flows, especially in the context of particle methods. In the latter a single-phase approximation is most usually adopted to reduce the computational costs and the model complexity. While it is well known that the role of the air largely affects the local flow evolution, it is still not clear whether this single-phase approximation is able or not to predict global flow features like the evolution of the global mechanical energy dissipation. The present work is dedicated to this topic through the study of a selected problem simulated both with single-phase and two-phase models. It is shown that, interestingly, even though flow evolutions are different, energy evolutions can be similar when including or not the presence of air. This is remarkable since, in the problem considered, with the two-phase model about half of the energy is lost in the air phase while in the one-phase model the energy is mainly dissipated by cavity collapses.

PACS numbers: 47.11.-j, 47.35.Bb, 47.10.ad, 47.32.-y

Keywords: free-surface flow, gravity waves, breaking waves, viscous dissipation, Smoothed Particle Hydrodynamics

*Electronic address: andrea.colagrossi@cnr.it

Introduction

In the last decades, the interest in free-surface flows has notably grown from both the scientific and the engineering points of view, the involved problems ranging from marine and coastal engineering fields. As is well known, this class of flows involves challenging phenomena to model and simulate because of the multiple fragmentations and reconnections of the air-water interface. Several numerical methods have been developed to date to tackle this problem; among them, two classes of methods gained vast popularity in the numerical community: mesh-based CFD (Computational Fluid Dynamics) solvers coupled with interface capturing techniques (Finite Volumes, Differences, Elements with Level Set or Volume of Fluid approaches) and Particle Methods (SPH, MPS). The former class, based on Eulerian grid, is currently applied in most of naval/coastal and marine engineering applications. On the other side, Particle Methods, thanks to their meshless Lagrangian character, have proven to be remarkably effective when dealing with large deformation and fragmentations/reconnections of the air-water interface.

Besides the general numerical scheme adopted, the preliminary choice that must be made when solving free-surface flows is related to the modelling of the gaseous phase. The density ratio between water and air being large ($\sim$ 820), in order to save computational resources and to simplify the numerical modelling, only the liquid phase is often modelled, the role of the gas being assumed negligible. Similarly, as the flow velocity is much smaller than the sound speed in water, the chosen model is often the incompressible approximation, density variation being therefore neglected. Nevertheless, when simulating complex free-surface flows, these choices are not at all obvious nor easily justified. The replacement of air with vacuum deprives the flow of cushioning mechanisms in cavities, which can significantly alter the dynamics of the flow and energy transfer processes. Moreover, when a vacuum cavity collapses, a discontinuous drop of mechanical energy occurs (see, *e.g.* 1) when the incompressible model is assumed. Conversely, in a weakly-compressible model the cavity collapse induces rapid exchanges between mechanical energy and internal (elastic) energy [2] which are dissipated in few cycles by numerical viscosity.

The objective of the present study is to address the implications of single-phase approximation on the simulation of energetic free-surface flows, with particular focus on energy evolution, transfer and dissipation. To this end, a Smoothed Particle Hydrodynamics (hereinafter SPH) solver is used. This solver was chosen because of its intrinsic conservation properties (mass, momenta and energy), the absence of numerical diffusion associated to advection (contrary to

Eulerian methods), and the accurate description of the interface also during large deformation and fragmentation (perfectly non diffusive interface). In Colagrossi et al. [3] an assessment methodology of the SPH method for free-surface flows in terms of energy evolution and dissipation was developed in a single-phase approximation context. It was validated and applied to viscous free-surface test-cases like the attenuation of a viscous standing wave or the evolution of a breaking wave in viscous flow. In the present work this analysis is extended to higher Reynolds number flow in a multiphase flow context.

The article is organised as follows:

- section I: the main features of complex free-surface flows involving breaking processes (multiple reconnections, fragmentations) are briefly re-called.
- sections II and III: the local governing equations for both single- and two-phase flows are presented, as well as the global energy balance in the single- or two-phase flow domain;
- section IV: a brief introduction of the SPH numerical model and energy balance for this particle system is given for multiphase flows;
- section V: analysis is made on the case of shallow water breaking wave. Attention is first focused on the processes driving the mechanical energy decay under single-phase approximation, and the role of free-surface deformation. For the lack of detailed experimental data, a cross-validation with an available single-phase Finite Volume Level-Set (LS-FVM) solver is provided. Then, the same test case is simulated using a two-phase SPH solver. The mechanical energy exchange between air and water is analysed, together with the possible reasons for energy dissipation during the plunging phase.

I. MAIN FEATURES OF ENERGETIC FREE-SURFACE FLOWS

The main complexity of energetic free-surface flows is linked to the reconnections of the free surface which induce circulation and vorticity injection inside the fluid (see, *e.g.*, [4, 5]), with the related vortical post-breaking behaviour (see, *e.g.*, [6]) where the air phase plays an important role.

The evolution of the air entrapped in cavities significantly depends on the pressure forces in the gaseous phase, and on their importance when compared with the inertia of the liquid phase. The non-dimensional parameter that properly represents this ratio is the Euler number defined as

Eu = $p_{0air}/(\rho_{water}U^2_{water})$. If Eu is large, the air phase has an influence and can be treated as an incompressible medium. Conversely in the limit of vanishing Eu, the process can be studied by a single-phase approximation, then neglecting the air cushion effect [7] which plays a minor role in that case. In the intermediate cases air needs to be modelled as a compressible medium and Eu represents there the stiffness of the entrapped air (see, *e.g.*, [8]). In the present study aiming at macroscopic complex free-surface flows (as those encountered in marine and coastal engineering), Eu has intermediate values and thus compressible modeling of the air phase must be adopted, as we do in the present work.

Another important physical effect in general free-surface flows is surface tension. Again, given the scales of the air-water flows at aim (involving typically breaking event sizes in the range 1m-10m), the finest space resolutions which can be used numerically nowadays are of the order of centimeters. It is therefore a sound assumption to neglect surface tension effects in this context. Note that this assumption does not hold for the smaller and smaller structures appearing in spray and degassing phases consequent to multiple breaking. Surface tension action on these structures is neglected in the present work and assumed to play a negligible role in the flow energy evolution, even though it its role is non-negligible locally.

These crucial aspects can raise doubts about the plausibility of the use of single-phase models (most often without surface tension modelling) for the prediction of energy dissipation during complex free-surface flow evolutions. Nevertheless several works addressing wave breaking under single-phase approximation can be found in the literature. Moreover, in works like the ones by, *e.g.*, Landrini et al. [9] and Bouscasse et al. [10, 11], even using a single-phase assumption the prediction of energy dissipation due to breaking is in line with both theoretical results and experimental measurements. An in-depth discussion on this issue is provided in the next sections.

II. GOVERNING EQUATIONS

A. Single phase model

Consider a liquid domain Ω_w delimited by its boundary, $\partial\Omega_w$, composed of a free surface, $\partial\Omega_F$ and a solid surface $\partial\Omega_B$. The liquid evolution can be modelled by a single-phase weakly-compressible model:

$$\begin{cases} \dfrac{D\rho}{Dt} = -\rho\,\mathrm{div}(\boldsymbol{u})\,, & \dfrac{D\boldsymbol{u}}{Dt} = \boldsymbol{g} + \dfrac{\mathrm{div}(\mathbb{T})}{\rho} \\ \dfrac{De}{Dt} = \dfrac{\mathbb{T}:\mathbb{D}}{\rho}\,, & \dfrac{D\boldsymbol{r}}{Dt} = \boldsymbol{u}, \qquad p = f(\rho)\,, \end{cases} \tag{1}$$

where D/Dt represents the Lagrangian derivative, $\boldsymbol{u}$ the flow velocity, $\boldsymbol{r}$ the position of the material points, ρ the fluid density, e the specific internal energy, $\mathbb{T}$ the stress tensor, $\mathbb{D}$ the rate of strain tensor and $\boldsymbol{g}$ is a generic specific body force. Thermal conductivity effects are here neglected, and the liquid is considered to be Newtonian:

$$\mathbb{T} = -p\mathbb{1} + 2\mu_w\,\mathbb{D}\,, \tag{2}$$

where μ_w is the dynamic viscosity of the liquid and where viscosity effects linked to the compressibility have been neglected; this is a usual approximation in the weakly-compressible regime (see, *e.g.*, 12).

The pressure p is considered to depend only on the density since for a liquid medium the effects of entropy/temperature on the pressure are generally negligible; moreover, in the weakly-compressible regime a simple linear equation of state can be used:

$$p = c_{0\,w}^2\,(\rho - \rho_{0\,w})\,, \tag{3}$$

where $c_{0\,w}$ is the speed of sound (assumed constant) of the liquid medium and $\rho_{0\,w}$ the density on the free-surface (where p is assumed equal to zero). The weakly-compressible regime (density variations smaller than $0.01\rho_{0\,w}$) is guaranteed when the pressure variations stay within the range:

$$\frac{\Delta\rho}{\rho_{0\,w}} < 0.01 \quad \Rightarrow \quad \frac{p}{c_{0\,w}^2\,\rho_{0\,w}} < 0.01\,. \tag{4}$$

In other word by properly defining a reference velocity of the problem U_w (see *e.g.* [2]) and a Mach number for the liquid phase as

$$\mathrm{Ma}_w := U_w/c_{0\,w}\,, \tag{5}$$

the fulfillment of the weakly-compressible assumption can be guaranteed if Ma_w remains always less than 0.1 during the time evolution. For numerical purposes $c_{0\,w}$ can thus be chosen smaller than its actual value to avoid too small time steps; however, the constraint $\mathrm{Ma}_w < 0.1$ has to be respected to remain in the weakly-compressible regime [13].

From the point of view of the dimensionless quantities the single phase model is governed by the Reynolds, the Froude and the Mach numbers:

$$\mathrm{Re}_w := \frac{\rho_{0\,w}\, U_w\, L}{\mu_w}\,, \qquad \mathrm{Fr}_w := \frac{U_w}{\sqrt{g\, L}}\,, \qquad \mathrm{Ma}_w := \frac{U_w}{c_{0\,w}}\,,$$

with L the reference length of the problem and g the gravity acceleration.

1. Boundary conditions

At the free surface both kinematic and dynamic boundary conditions must be satisfied. The kinematic free-surface boundary condition implies that, while evolving with the fluid flow, the material points initially on $\partial\Omega_F$ remain on it. This condition fails to hold when reconnections of the free surface occur (e.g., when a plunging breaking wave impacts on the free surface). The dynamic free-surface boundary condition expresses the continuity of stress across the free surface. In this work we assume surface tension effects to be negligible. As a consequence, zero stresses act at the free surface.

As far as solid surfaces are concerned, in this work simple free-slip boundary conditions are adopted, in order to avoid dissipations due to solid walls, making easier the monitoring of the dissipation in the complex free-surface flows studied here.

B. Two-phase model

We now consider a two-phase domain Ω composed of a liquid domain, Ω_{water}, and a gas domain, Ω_{air} (*i.e.* $\Omega = \Omega_{water} \cup \Omega_{air}$). The system of equations 1 is valid in each phase Ω_{water} and Ω_{air}, and the mutual interaction across the liquid-gas (water-air in our context) interface need to be modelled. Following Zapryanov and Tabakova [14] and assuming that surface-tension effects can be neglected , on the air-water interface the stress vector is continuous:

$$(\mathbb{T}\cdot\boldsymbol{n})_{water}(\boldsymbol{r}) = (\mathbb{T}\cdot\boldsymbol{n})_{air}(\boldsymbol{r}) \qquad \forall \boldsymbol{r} \in \partial\Omega_{water} \cap \partial\Omega_{air}\,. \tag{6}$$

This dynamic condition needs to be combined with a kinematic condition for the interface motion, which ensures the continuity of the velocity field.

To model the air phase the following polytropic equation of state is used:

$$p \;=\; P_{0\,air}\left(\frac{\rho}{\rho_{0\,air}}\right)^{\gamma_{air}} \qquad \Rightarrow \qquad c^2_{0\,air} \;=\; \frac{P_{0\,air}\,\gamma_{air}}{\rho_{0\,air}}\,, \tag{7}$$

where $\rho_{0\,air}$ is the air density at rest, $\gamma_{air} = 1.4$ is the air adiabatic index, and finally $P_{0\,air}$ is the air ambient pressure.

Differently from the single-phase model, the speed of sound $c_{0\,air}$ can not be adjusted for computational convenience, as in the the case of $c_{0\,water}$. Indeed, we are interested in simulating flows where the air phase can be entrapped by the water phase during impact events. Considering the model for compression of an air-pocket by a plunging water jet proposed by [15] the maximum density $\rho_{air}^{\mathrm{Max}}$ in the entrapped air pocket follows the scaling law:

$$\rho_{air}^{\mathrm{Max}} \propto \left(\frac{1}{\sqrt{Eu}}\right)^{1/\gamma_{air}} = \left(\mathrm{Ma}_{air}\sqrt{\frac{\gamma_{air}\,\rho_{0\,water}}{\rho_{0\,air}}}\right)^{1/\gamma_{air}}, \qquad \mathrm{Ma}_{air} := \frac{U_{water}}{c_{0\,air}}, \tag{8}$$

where we assumed that the reference velocity for the air phase is the same used for the water phase. In coastal/naval engineering problems, from model to real scale the Eu number varies within the range (100 - 1) and, therefore, even if Ma_{air} is less than 0.1, the weakly compressible regime (density variations less than 1%) is not guaranteed in the air phase. Thus, the real value of $c_{0\,air}$ has to be adopted in the model to take into account the possible non-negligible compressibility effects. This aspect is rarely discussed in the literature of breaking waves. The adoption of the real value of $c_{0\,air}$ implies small time steps when solving explicitely the system (1), and the CPU costs can thus be rather high even in a 2D framework. It is worth mentioning that the scaling law (8) has been numerically verified for shallow water breaking wave in [7] using a two-phase SPH model.

Finally, from the point of view of the dimensionless quantities the two-phase model is governed by:

$$\mathrm{Re}_{water}\,,\mathrm{Fr}_{water}\,,\mathrm{Ma}_{water}\,,\left(\frac{\mu_{air}}{\mu_{water}}\right),\left(\frac{\rho_{0\,air}}{\rho_{0\,water}}\right),\mathrm{Eu}\,,\gamma_{air}\,, \tag{9}$$

where the Weber/Bond number is omitted being the surface tension effects not considered in the present work.

III. DISSIPATION OF MECHANICAL ENERGY

The mechanical energy of the fluids $\mathcal{E}_M$ is given by the sum of the kinetic $\mathcal{E}_K$ and potential energy $\mathcal{E}_P$. Assuming that no external non-conservative forces are present, and that the solid surfaces $\partial\Omega_B$ are not moving, the time variation of $\mathcal{E}_M$ is given by:

$$\dot{\mathcal{E}}_M = \int_\Omega \mathrm{div}\,(\mathbb{T})\cdot\boldsymbol{u}\,\mathrm{d}V\,. \tag{10}$$

Applying the divergence theorem, the mechanical power $\mathcal{P}_{\partial\Omega/fluid}$, acting on the fluids on their boundaries $\partial\Omega$, can be expressed as:

$$\mathcal{P}_{\partial\Omega/fluid} = \int_{\partial\Omega} (\boldsymbol{n}\cdot\mathbb{T})\cdot\boldsymbol{u}\,\mathrm{d}S = \int_{\Omega} \mathrm{div}(\mathbb{T})\cdot\boldsymbol{u}\,\mathrm{d}V + \int_{\Omega} \mathbb{T}:\nabla\boldsymbol{u}\,\mathrm{d}V\,, \tag{11}$$

$\boldsymbol{n}$ being the outward unit normal vector. The surface integral is zero on $\partial\Omega_B$, since the forces on the solid surfaces are not doing mechanical work on the fluid media. When considering a two phase model, $\partial\Omega \equiv \partial\Omega_B$; conversely, with a single phase model, $\partial\Omega = \partial\Omega_B \cup \partial\Omega_F$. However, the power $\mathcal{P}_{\partial\Omega/fluid}$ is still zero on $\partial\Omega_F$ if surface tension effects are neglected. Therefore for both the models, by taking into account the symmetry of the stress tensor it is possible to write:

$$\dot{\mathcal{E}}_M = -\int_{\Omega} \mathbb{T}:\mathbb{D}\,\mathrm{d}V\,. \tag{12}$$

A. Single phase model

Let us consider the single phase model first, with constitutive law (2). Equation (12) can be rewritten as:

$$\dot{\mathcal{E}}_M + \dot{\mathcal{E}}_C = -2\mu_w \int_{\Omega} \mathbb{D}:\mathbb{D}\,\mathrm{d}V\,, \tag{13}$$

$\mathcal{E}_C$ being a pure reversible elastic energy, linked to the weak compressibility. Its expression depends on the equation of state adopted (see, *e.g.*, 2); in our case it is:

$$\mathcal{E}_C = \mathcal{E}_C(\rho_0) + c_0^2 \int_{\Omega} \left[\log\left(\frac{\rho}{\rho_0}\right) + \frac{\rho_0}{\rho} - 1 \right] \rho\,\mathrm{d}V\,. \tag{14}$$

The right hand side of (13) is the power dissipated by viscosity:

$$\mathcal{P}_V := -\int_{\Omega} \epsilon_V\,\mathrm{d}V\,, \qquad \epsilon_V := 2\mu_w\,\mathbb{D}:\mathbb{D}\,, \tag{15}$$

ϵ_V being the volume-specific viscous dissipation power. Time integration of $\mathcal{P}_V$ yields the viscous heating Q_V.

The elastic energy $\mathcal{E}_C$ is null for an incompressible medium. If in addition the fluid is also inviscid, the energy balance (13) can not be satisfied anymore during impact events, and instantaneous energy loss must take place (see, *e.g.*, 1, 2). In that case the energy balance has to be rewritten as:

$$\dot{\mathcal{E}}_M - \dot{\mathcal{E}}_\Delta = 0\,, \tag{16}$$

where the time variation $\dot{\mathcal{E}}_\Delta$ must behave as a Dirac *delta* function:

$$\dot{\mathcal{E}}_\Delta(t) \;=\; \sum_l K_l \delta(t - t_l^\star)\,. \tag{17}$$

This term is non-zero only during collisions of liquid surfaces and/or during liquid/solid impacts, taking place at a finite number of time instants $t = t_l^\star$. The intensities K_l are unknowns, as they depend on the kinematics and geometric configuration of the impinging liquid surfaces.

For an inviscid weakly-compressible flow, the elastic energy $\mathcal{E}_C$ is generally not negligible during fluid-fluid or fluid-solid impact events [16]. $\mathcal{E}_C$ is characterised by high frequency acoustic components and this energy is exchanged with the mechanical energy $\mathcal{E}_M$ with time cycles whose duration depends on the speed of sound c_w. These pressure oscillations, if not properly handled, represent an issue. As theoretically found by Cooker [17], and shown in Marrone et al. [2] by numerical simulations, once these acoustic components are dissipated the value of the residual mechanical energy $\mathcal{E}_M$ is close to the incompressible flow solution, the dissipated elastic energy being quite close to $\mathcal{E}_\Delta$. This is due to the fact that in the weakly-compressible regime the solution of the compressible Euler equation can be approximated with the solution of an incompressible medium plus a superimposition of an acoustic component (see e.g. 18).

B. Two phase model

When considering the two fluid domains Ω_{air} and Ω_{water}, eq. (13) becomes:

$$\begin{cases} (\dot{\mathcal{E}}_M + \dot{\mathcal{E}}_C)_{water} + (\dot{\mathcal{E}}_M + \dot{\mathcal{E}}_C)_{air} = \mathcal{P}_{V\,water} + \mathcal{P}_{V\,air} \\ \mathcal{P}_{V\,water} := -2\,\mu_{water} \displaystyle\int_{\Omega_{water}} \mathbb{D} : \mathbb{D}\,\mathrm{d}V\,, \qquad \mathcal{P}_{V\,air} := -2\,\mu_{air} \int_{\Omega_{air}} \mathbb{D} : \mathbb{D}\,\mathrm{d}V\,. \end{cases} \tag{18}$$

The viscous heats $\mathcal{Q}_{V\,water}$ and $\mathcal{Q}_{V\,air}$ are obtained by time integration of their respective powers $\mathcal{P}_{V\,water}$ and $\mathcal{P}_{V\,air}$.

Once integrated in time, the terms of equation (18) can be rearranged as:

$$\begin{cases} \mathcal{L}_{air/water} = (\Delta\mathcal{E}_M + \Delta\mathcal{E}_C)_{water} - \mathcal{Q}_{V\,water} \\ \mathcal{L}_{water/air} = (\Delta\mathcal{E}_M + \Delta\mathcal{E}_C)_{air} - \mathcal{Q}_{V\,air} \\ \mathcal{L}_{air/water} + \mathcal{L}_{water/air} = 0\,. \end{cases} \tag{19}$$

$\mathcal{L}_{water/air}$ being the work done by water on the air phase and $\mathcal{L}_{air/water}$ the work done by air on the water phase. In system (19) we adopted the notation:

$$\Delta\mathcal{E}_{Xy} := \int_0^t \dot{\mathcal{E}}_{Xy}\,\mathrm{d}t\,.$$

The main difference with the single phase model is that now, in the collisions of liquid or liquid/solid surfaces, the gaseous phase initially separates those surfaces.

In terms of energy components, in the two-phase model we have that:

I) differently from the single-phase model, $\Delta\mathcal{E}_{C_{water}}$ plays a minor role since liquid-liquid impacts are attenuated by the entrapped gas bubbles. This term is generally negligible, as confirmed by the numerical simulations shown in the following;

II) because of the very small air–to–water density ratio, $\Delta\mathcal{E}_{M\,air}$ is negligible with respect to $\Delta\mathcal{E}_{M\,water}$;

III) $\Delta\mathcal{E}_{C\,air}$, i.e. the energy term related to air-cushion phenomena, strongly depends on the Euler number and is linked to air bubble oscillations, characterised by high frequency components. In the numerical simulations performed in this work, $\Delta\mathcal{E}_{C\,air}$ remains always negligible with respect to $\Delta\mathcal{E}_{M\,water}$, though the air compressibility can strongly affect the pressure field and the related flow evolution.

From the above considerations, the system (19) can be simplified as:

$$\begin{cases} \mathcal{L}_{air/water} \approx \Delta\mathcal{E}_{M\,water} - \mathcal{Q}_{V\,water} \\ \mathcal{L}_{water/air} \approx -\mathcal{Q}_{V\,air} \\ \mathcal{L}_{air/water} + \mathcal{L}_{water/air} = 0 \Rightarrow \Delta\mathcal{E}_{M\,water} \approx (\mathcal{Q}_{V\,water} + \mathcal{Q}_{V\,air}) \,. \end{cases} \tag{20}$$

Therefore, $\Delta\mathcal{E}_{M\,water}$ is likely to decrease monotonically, with a time derivative very close to $(\mathcal{P}_{V\,water} + \mathcal{P}_{V\,air}) \leq 0$. The ratio between the two viscous heating $\mathcal{Q}_{V\,water}$, $\mathcal{Q}_{V\,air}$ is *a priori* unknown. For example, in the 3D breaking wave simulated by Lubin et al. [19], the authors find that the main dissipation mechanism is linked to the motion of the entrapped air bubbles, which implies that $\mathcal{Q}_{V\,water}$ is dominant. Conversely, in the recent work of Iafrati et al. [20], where the dynamics of the modulational instability of 2D free surface waves is studied, it has been observed that, during breaking events, large dipole structures in the air phase are generated, with values of $\mathcal{Q}_{V\,air}$ larger than $\mathcal{Q}_{V\,water}$.

Therefore, it seems that the ratio between these two components is problem-dependent and deserves more in-depth investigation. Furthermore, in Iafrati et al. [20] it is clearly shown that numerical difficulties arise in achieving converged values for the two components $\mathcal{Q}_{V\,water}$ and $\mathcal{Q}_{V\,air}$, even in a two-dimensional framework. This is probably related to the fact that large velocity

gradients are very localised in time and space, as further discussed in the next sections. This is the main reason why, in the following, our work is limited to 2D cases, seeking to obtain converged results from which to draw as reliable as possible conclusions. The attainment of converged results on similar 3D complex free-surface flows is actually beyond current computational capabilities.

IV. NUMERICAL MODEL

A brief introduction on the adopted SPH scheme is given in this section. As described in section II, the weakly-compressible model described is adopted for the liquid phase, while air is treated as a compressible medium so that air-cushion effects can be properly accounted for [7]. Given a set of particles, each characterised by its own mass m_i, velocity u_i and position $\boldsymbol{r_i}$, and belonging to a specific phase, the set of governing equations (1) can be discretized, in the SPH framework, as:

$$\begin{cases} \dot{\rho}_i(t) = -\rho_i \displaystyle\sum_j \frac{m_j}{\rho_j}(\boldsymbol{u}_j - \boldsymbol{u}_i)\cdot\nabla_i W_h \\ \dot{\boldsymbol{u}}_i(t) = -\displaystyle\sum_j \frac{m_j}{\rho_i\rho_j}(p_j + p_i)\nabla_i W_h + \sum_j \left(\frac{2\mu_i\mu_j}{\mu_i+\mu_j}\right)\frac{m_j}{\rho_i\rho_j}\pi_{ij}\nabla_i W_h + \boldsymbol{g}_i \\ \dot{e}_i(t) = -p_i \displaystyle\sum_j \frac{m_j}{\rho_i\rho_j}(\boldsymbol{u}_j - \boldsymbol{u}_i)\cdot\nabla_i W_h + \sum_j \left(\frac{\mu_i\mu_j}{\mu_i+\mu_j}\right)\frac{m_j}{\rho_i\rho_j}\pi_{ij}(\boldsymbol{u}_j - \boldsymbol{u}_i)\cdot\nabla_i W_h \\ \dot{\boldsymbol{r}}_i(t) = \boldsymbol{u}_i(t)\,, \\ p_i = c_{0\,water}^2\,(\rho_i - \rho_{0\,water}) + P_{bg} \qquad \text{if } i \in \text{water}\,, \\ p_i = \dfrac{c_{0\,air}^2\rho_{0\,air}}{\gamma_{air}}\left[\left(\dfrac{\rho_i}{\rho_{0\,air}}\right)^{\gamma_{air}} - 1\right] + P_{bg} \qquad \text{if } i \in \text{air}\,, \end{cases} \tag{21}$$

where ρ_i, p_i and e_i are, respectively, the density, pressure and internal energy, of the i-th particle. The positive constant pressure P_{bg} is used to ensure that the pressure field is always greater than zero in order to avoid the so-called *tensile instability*. The *kernel* function $W_h = W_h(\boldsymbol{r}_i - \boldsymbol{r}_j)$ is a positive, smooth approximation of the Dirac delta function W. The symbol ∇_i indicates differentiation with respect to the position of the i-th particle. W_h has a compact support of radius $2h$, h being the *smoothing length* in the SPH literature. The viscous stresses are modelled through the formula by Monaghan and Gingold [21]:

$$\pi_{ij} = 2\,(n+2)\,\frac{(\boldsymbol{u}_j - \boldsymbol{u}_i)\cdot(\boldsymbol{r}_j - \boldsymbol{r}_i)}{\|\boldsymbol{r}_j - \boldsymbol{r}_i\|^2}\,, \tag{22}$$

where n is the number of spatial dimensions of the problem at hand. Thanks to the symmetric structure of equations (21) the exact momentum and energy conservations of the system are guaranteed (see, e.g., 22).

For simple domain geometries the fluid particles can be initially positioned on a regular lattice; at the initial instant all particles have the same volume, namely V_0, which is equal to the fluid domain volume divided by the number of fluid particles. Consistently, the particle mean spacing is denoted by $\Delta x = V_0^{1/n}$. Along with the volume distribution, the initial pressure, velocity and mass of the particles are prescribed. For $h \to 0$ and $\Delta x/h \to 0$, the system (21) is consistent with the Navier-Stokes equations (see, e.g., 23).

Concerning the internal energy equation in (21), the two terms on the right-hand-side are linked, respectively, to the power components $\mathcal{P}_C$ and $\mathcal{P}_V$ defined in (15):

$$\begin{cases} \mathcal{P}_C^{\text{SPH}} = -\sum_i \sum_j \dfrac{m_i m_j}{\rho_i \rho_j} p_i (\boldsymbol{u}_j - \boldsymbol{u}_i) \cdot \nabla_i W_h \\ \mathcal{P}_V^{\text{SPH}} = -\sum_i \sum_j \left(\dfrac{\mu_i \mu_j}{\mu_i + \mu_j} \right) \dfrac{m_i m_j}{\rho_i \rho_j} \pi_{ij} (\boldsymbol{u}_j - \boldsymbol{u}_i) \cdot \nabla_i W_h \,. \end{cases} \tag{23}$$

Furthermore, for the liquid phase, substituting the equation of state (3) and using the continuity equation in $\mathcal{P}_C^{\text{SPH}}$, after some algebraic manipulations it is possible to recover the equation (14) at the discrete level:

$$\mathcal{P}_C^{\text{SPH}} = \dot{\mathcal{E}}_C^{\text{SPH}}, \qquad \mathcal{E}_C^{\text{SPH}} = \mathcal{E}_C^{\text{SPH}}(\rho_{0\,water}) + c_{0\,water}^2 \sum_i m_i \left[\log\left(\frac{\rho_i}{\rho_{0\,water}} \right) + \frac{\rho_{0\,water}}{\rho_i} - 1 \right], \tag{24}$$

and the same procedure can be repeated for the air phase using the equation of state (last equation of 21).

Thanks to the Lagrangian formulation the enforcement of the kinematic free-surface boundary conditions is intrinsically satisfied. For the single-phase model the dynamic free-surface boundary is also intrinsically satisfied in the present SPH model since work done by the stresses on the free-surface is zero as shown in Colagrossi et al. [23, 24] .

Note that any two-phase SPH model naturally keeps the air-water interface sharp [7, 25, 26] due to its Lagrangian nature, and also preserves exactly the mass of each phase, being a particle method. Also, the dynamic boundary condition (6) at the interface is intrinsically satisfied in a smoothed sense, thanks to the symmetry of the particle-particle interactions.

For the enforcement of boundary conditions on solid surfaces, since in this work only flat surfaces are considered, the simple classical ghost-fluid approach is adopted (see 7).

The above SPH schemes have been widely validated in the past years for both single and two-phase models on several benchmark test-cases. In particular in [7, 25, 26] the two-phase SPH model has been used to simulate bubbly-flow evolution comparing the SPH outputs with reference solutions. The convergence of the scheme has been also heuristically verified through dedicated tests changing the spatial/time resolutions.

Concerning the time integration, a 4th-order Runge-Kutta scheme is used. For the simulations presented in this article the acoustic constraint is always the most restrictive (for more details see *e.g.* [27])

$$\Delta t \leq K_a \frac{(2\,h)}{c_{0X}}\,, \tag{25}$$

where $2h$ is the Kernel radius, K_a is the Courant-Friedrichs-Lewy constant which depends on the specific time integrator (in the present case K_a is equal to 0.75) and c_{0X} is the speed of sound in the generic phase X. When considering the two-phase model, as stated in section II B, the numerical sound speed in the air phase must be the physical one, $c_{0\,air} = 343\,m/s$ (with ambient temperature and pressure conditions), which implies very small time steps.

A. SPH model with numerical diffusive terms

As the PDEs (21) are integrated in time with an explicit scheme and as the spatial differential operators are spatially centred with respect to the particle position, the SPH scheme develops non-physical pressure oscillations at high frequency. This is a well-known issue in the literature, see, e.g., [28, 29]. To cope with this problem, in the present work the δ-SPH scheme is adopted. This variant of the classical SPH scheme is a derivation from Riemann-based SPH solvers and is characterised by the use of an additional diffusive term in the continuity equation aimed at removing the acoustic noise in the pressure field, while preserving a proper treatment of the free-surface [30]. Because of the additional numerical diffusion introduced in that case, a further energy component $\mathcal{P}_N^{\text{SPH}}$ appears in eq. (13):

$$\dot{\mathcal{E}}_M^{\text{SPH}} + \dot{\mathcal{E}}_C^{\text{SPH}} = \mathcal{P}_V^{\text{SPH}} + \mathcal{P}_N^{\text{SPH}}\,. \tag{26}$$

This term $\mathcal{P}_N^{\text{SPH}}$ is consistent (it tends to zero when increasing the spatial resolution) and can be exactly quantified [31]. In spite of the introduction of an artificial diffusive term, when treating inviscid flows this scheme allows for a better mechanical energy conservation with respect to

the standard SPH one, where part of the mechanical energy is converted into non-physical high frequency components of $\mathcal{E}_C$ [31].

V. NUMERICAL SOLUTIONS OF A SHALLOW WATER BREAKING WAVE

In this section a violent shallow water flow is considered, characterized by the formation of a large plunging jet and by the presence of multiple breaking events. A possible way to generate such a flow is to create an intense breaking wave by using a moving piston in shallow water condition; however, such a generation would add the complexity of taking into account the mechanical work done by the piston on the fluid. Instead, we generate such a large plunging breaker and consequent multiple breaking events by means of a confined dam-break flow.

Indeed, this complex free-surface flow generation represents an ideal candidate for the analysis to be carried out, the flow being characterised by clearly identifiable stages, each with a peculiar dissipation mechanism:

I) inviscid fluid deformation,

II) water impact on a vertical wall,

III) backward plunging jet formation,

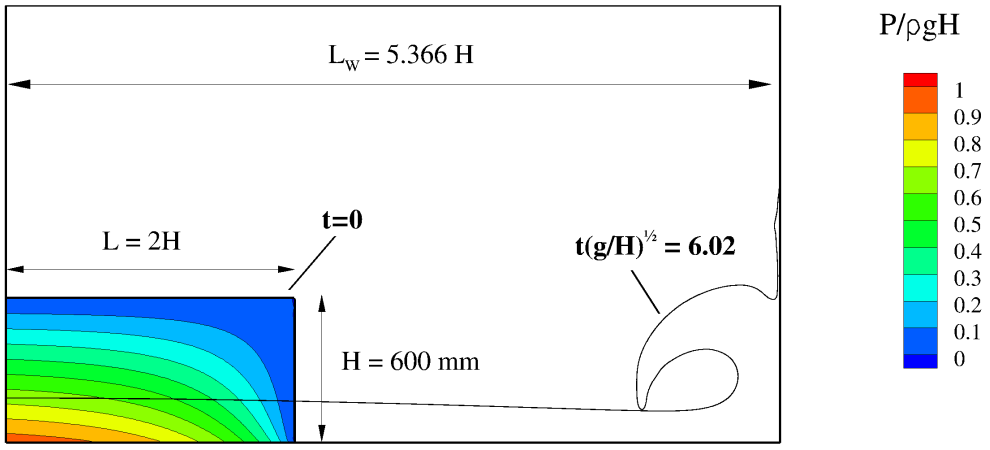

FIG. 1: Sketch of the confined dam-break flow problem. Contours are representative of the pressure field in the initial configuration.

IV) splashing stage with several cycles,

V) final sloshing flow regime,

VI) back to calm water.

This test has been extensively used in the literature (see, *e.g.*, 7, 32, 33, 34, 35) and good comparisons with experimental measurements have been obtained using different SPH models.

During stage (iii) a large plunging jet is formed which can be properly discretized reducing numerical uncertainties with respect to other possible test cases. Because of this large plunging breaker an energetic breaking flow then develops, during which evolution the different energy components are recorded and analysed.

Figure 1 depicts a sketch of the problem: H indicates the initial height of the dam and is used as reference length scale for the problem, while $U_{water} = \sqrt{gH}$ is used as reference velocity. In Figure 1 the free surface configuration at time $t(g/H)^{1/2} = 6.02$ is also depicted in order to show that the plunging jet has a $O(H)$ characteristic length.

First row of table I reports the main dimensionless numbers at the model scale. On the second row the ones used in the SPH simulations. Because of numerical constraints the Re_{water} as well as Ma_{water} need to be modified. Regarding the latter, in section II A it has been already explained that the numerical speed of sound of water is decreased in order to avoid too small time steps. However, since Ma_{water} is less than 0.1 the weakly-compressible regime is still guaranteed for the liquid phase.

	Fr_{water}	Re_{water}	Ma_{water}	μ_{air}/μ_{water}	ρ_{air}/ρ_{water}	Eu	γ_{air}
Model Scale	1	$1.5\,10^{6}$	$1.6\,10^{-3}$	10^{-2}	10^{-3}	17.2	1.4
SPH	1	$\mathbf{5\,10^{3}}$	$\mathbf{10^{-2}}$	10^{-2}	10^{-3}	17.2	1.4

TABLE I: Dimensionless parameters at model scale (top row) and the ones used in the numerical simulations (bottom row). On the left part of the table the three parameters used in the single-phase model; on the right the additional four numbers needed in the two-phase model.

Concerning the Reynolds number, it is defined as $Re_H = H\sqrt{gH}/\nu$ and is here kept fixed and set equal to 5000. Note that the Reynolds number based on H is comparable to much higher Reynolds numbers based on, e.g., the wave length or other horizontal characteristic lengths as in, e.g., Iafrati [36] where $\mathrm{Re}_\lambda = O(10^5)$ (λ being the wave length) is equivalent to $\mathrm{Re}_H = 3000$. With this choice

of Re_H all the main vortex scales can be resolved through a SPH direct numerical simulation, attaining the convergence of the viscous dissipation Q_V with a number of particles of $O(10^6)$ (in a two-dimensional framework). Therefore, in this way turbulence models can be avoided thus simplifying the analysis. For the chosen Re, the viscous effects are small enough not to mar the inertial character of the plunging breaking waves of the test case. Indeed, the obtained solutions are very close to the inviscid ones presented in the literature, in terms of fluid deformation and pressure loads [32].

In the initial condition, the liquid is at rest and has only potential energy. The final configuration is the one with the fluid at rest filling the tank width. Therefore, the potential energy difference between these two configurations can be used as characteristic total energy of the problem:

$$\Delta\mathcal{E}_P \;=\; \mathcal{E}_{M0} - \mathcal{E}_{M\infty} \;=\; \rho\, g\, H^3 \left[1 \;-\; \frac{2H}{L_W}\right]. \tag{27}$$

In the next section as a first analysis, the problem is studied in the single-phase approximation. The SPH solver is cross-validated against an incompressible single-phase Level-Set Finite Volume method (LS-FVM). Then, in section V B the two-phase SPH model is adopted in order to highlight the differences and limits of the single-phase approximation and investigate the effect of the presence of air in the wave breaking dissipation.

A. Single-phase approximation solution

In figures 2 and 3 the time evolution of the confined dam-break flow problem is shown for both the SPH and LS-VFM solutions. The contour plots refer to the pressure fields. The maximum resolution used in the single-phase SPH solver is $H/\Delta x = 800$ (corresponding to 1,280,000 fluid particles). For the LS-FVM solver, used for cross-validation, the maximum spatial resolution was limited to $H/\Delta x = 400$, corresponding to about 1,300,000 mesh nodes, with a uniform discretisation of the whole tank.

The two solvers predict similar flow evolutions and pressure fields. Because the weakly-compressible regime is adopted in the SPH model, some travelling acoustic waves can be recognised in figure 3. However, the global pressure patterns obtained by the two solvers are quite similar, especially for the plots presented in figure 2. Larger discrepancies are visible in figure 3 where a small time shift can be also recognised.

In the initial stage, the water column collapses and the resulting flow impacts the right wall.

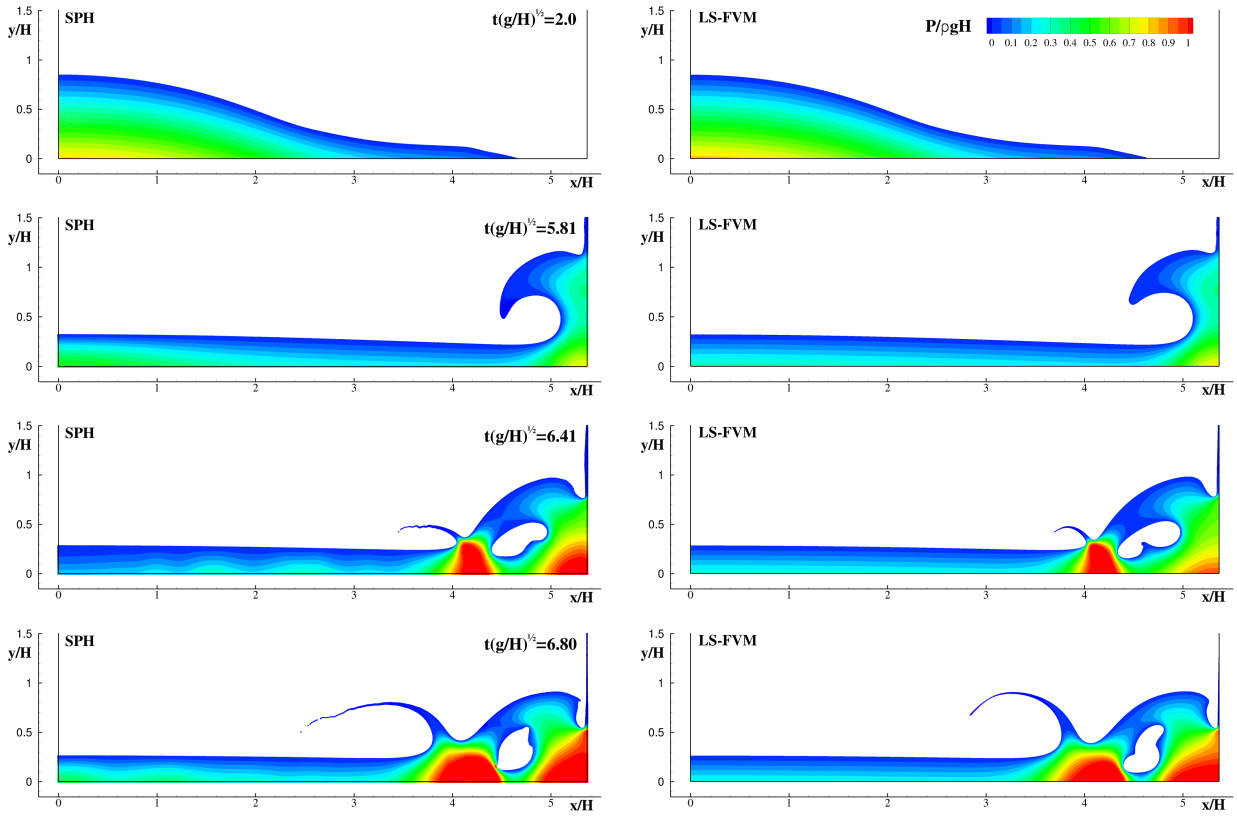

FIG. 2: Confined dam-break flow: comparison between SPH (left column) and LS-FVM (right column) solvers for the time instants $t\sqrt{g/H} = 2.0, 5.8, 6.2, 6.8$. Contours are representative of the pressure field. (Single-phase model).

During this stage the viscous effects are negligible, the flow being practically irrotational (first row of figure 2). Then a plunging wave is formed (second row of figure 2). This inviscid stage ends with the plunging closure ($t\sqrt{g/H} = 6.0$) followed by a complex splash-up stage (third and fourth rows of figure 2). In actual flows, starting from this instant the air phase plays a relevant role, as discussed in the next section. Under single-phase approximation, instead, an empty cavity is formed, whose volume reduces as the plunging jet enters the flow bulk and splashes up (first row of figure 3).

Due to the limited water depth, the splash-up feeds an upwelling water column which reaches a height larger than H. From this water column a fast thin jet is released, that hits the left vertical wall at time $t\sqrt{g/H} = 8.0$ (first row of figure 3). Because of the high kinetic and potential energy content of this jet (about 10% of the initial mechanical energy $\mathcal{E}_{M0}$), it plays a non-negligible role in the dissipation mechanism, as shown in the following. At later time, the volume cavity reduction goes on, until its collapse induces a violent fluid-fluid impact at about $t\sqrt{g/H} = 8.4$ (second row

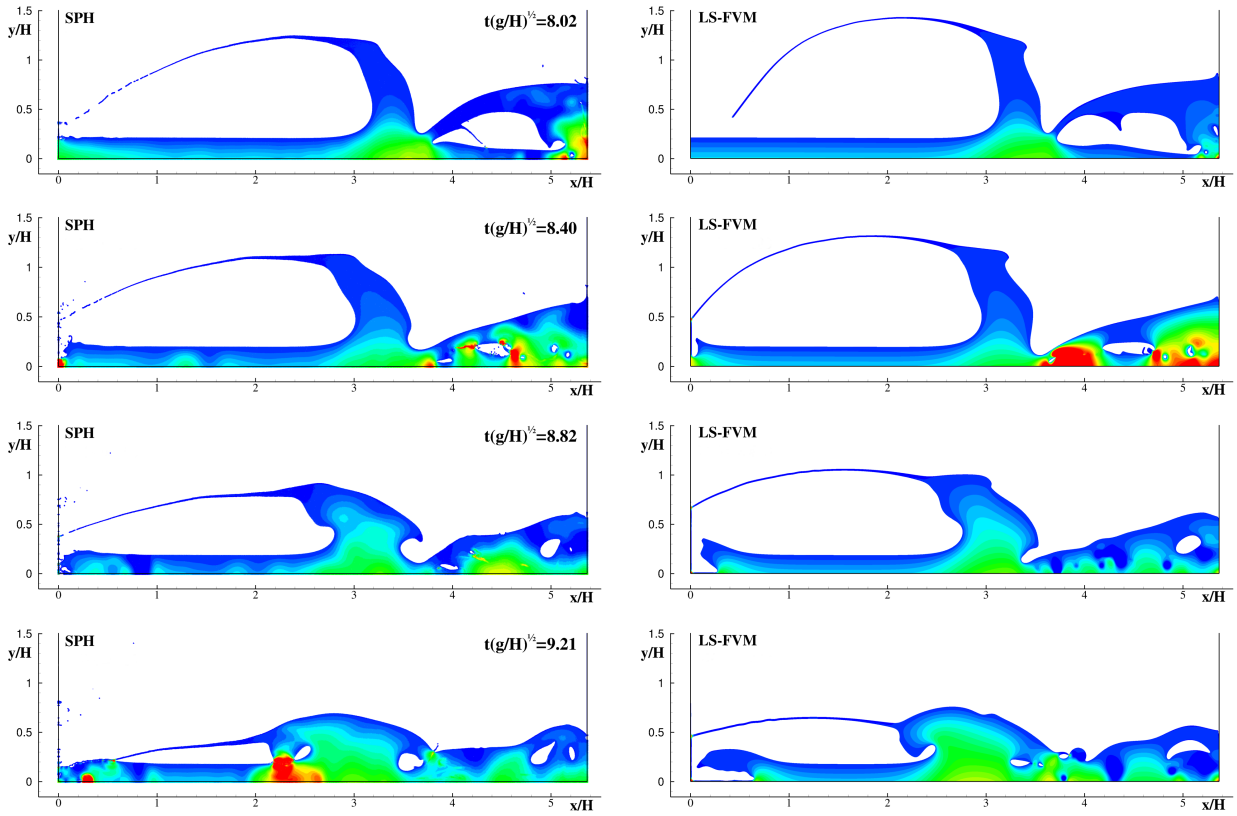

FIG. 3: Confined dam-break flow: comparison between SPH (left column) and LS-FVM (right column) solvers for the time instants $t\sqrt{g/H} = 8.0, 8.4, 8.8, 9.2$. Contours are representative of the pressure field. (Single-phase model).

of figure 3).

After the cavity closure, the water column originated by the first splash-up starts to collapse under the action of gravity, in the form of a mushroom-like structure, forming a backward-facing jet and a further plunging jet almost in the middle of the domain (third and fourth rows of figure 3). This kind of dynamics is very similar to the ones discussed by Bonmarin [37] for deep water breaking waves and by Landrini et al. [9] for breaking bores. However, in the present case, because of the shallow water regime, the vortical structures originated by the different breaking events cannot freely move below the free surface and remain confined and squashed in a limited water depth.

Figure 4 depicts the time history of the mechanical energy recorded with the two solvers. In the plot, the initial potential energy $\mathcal{E}_{M0}$ has been subtracted to $\mathcal{E}_M$ which is then made non-dimensional with the reference energy $\Delta\mathcal{E}_P$ (see eq. 27). Until the plunging jet formation ($t\sqrt{g/H} = 6.0$) the dissipation is practically zero as expected. During the splash-up, before the

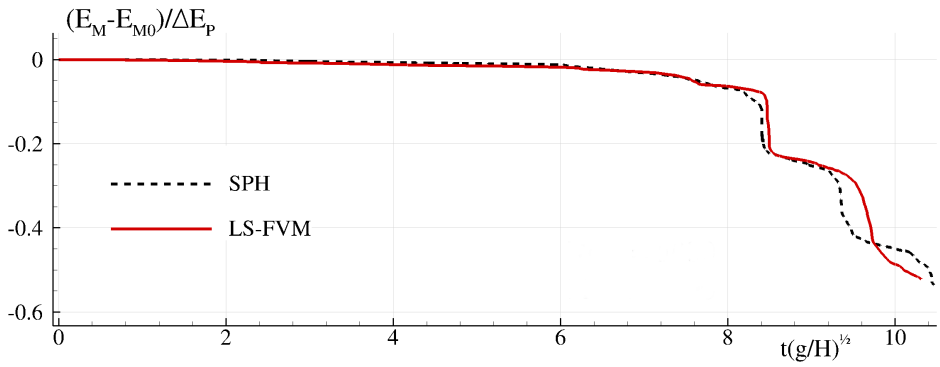

FIG. 4: Time histories of the mechanical energy evaluated by SPH and LS-FVM solvers. (Single-phase model).

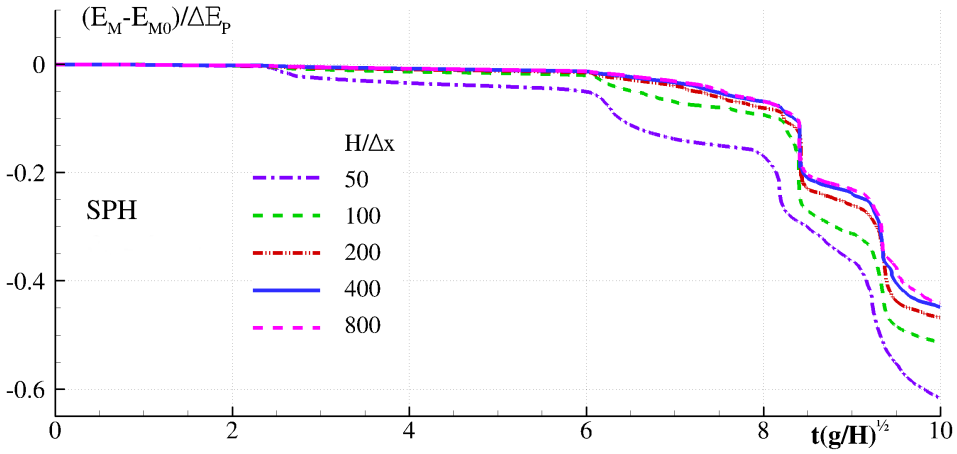

FIG. 5: Time histories of the SPH mechanical energy with varying the spatial resolution. (Single-phase model).

cavity closure, about 10% of the mechanical energy has been dissipated by the viscosity, whereas, just after the cavity closure, almost another 15% of the mechanical energy is dissipated in a very short time range because of the fluid-fluid impact. Remarkably, both the incompressible and the weakly-compressible models predict a similar energy drop, as introduced in section III.

After this stage, the flow becomes quite complex because of the vortical structures generated and because of the secondary splash-up stage; therefore, the dissipation process cannot be associated to particular events and, in addition, the time histories of the mechanical energy predicted by the two solvers starts to depart, although the magnitude of the predicted dissipation remains close. At time $t\sqrt{g/H} = 10.0$ both solvers predict a dissipation of about 50% of $\Delta\mathcal{E}_P$.

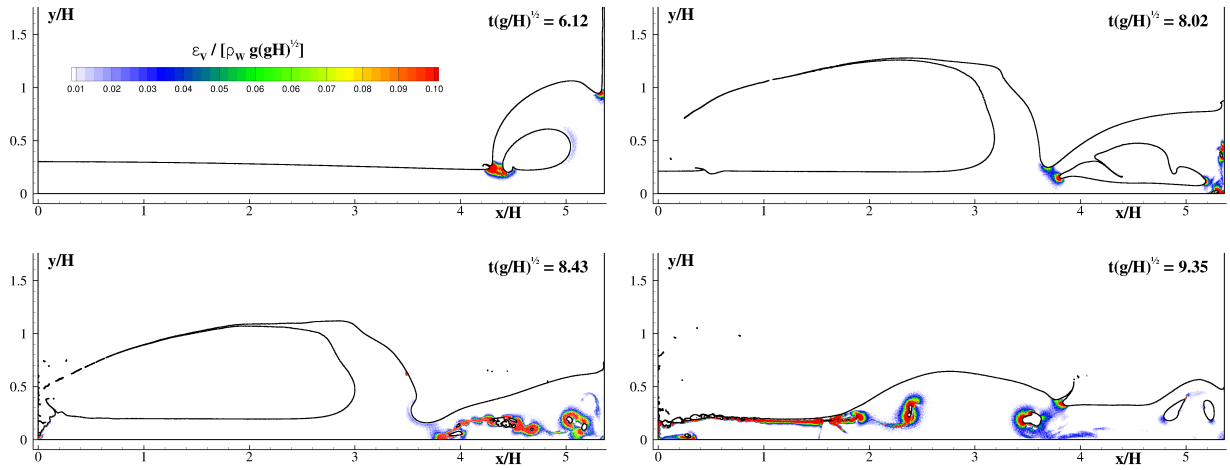

FIG. 6: Contour of the volume-specific dissipation ϵ_V (see eq. 15) for four time instants at Re=5000 using a spatial resolution $H/\Delta x = 800$. (Single-phase model).

This value is close to the one reported in Iafrati [36], where a comparable Re_H is used (of 3000) as mentioned above.

Figure 5 shows the time histories of the SPH mechanical energy, obtained with different spatial resolutions. A clear convergence of $\mathcal{E}_M$ is observed with an almost superimposition of the two highest resolution results.

In figure 6 the volume-specific viscous dissipation field ϵ_V is reported, in order to show the regions where viscous dissipation plays a major role. The last two time instants reported are the ones where the power $\mathcal{P}_V$ (see eq. 15) presents the highest values. They correspond to the cavity closure instant $t(g/H)^{1/2} = 8.43$, already commented above, and to the collapse of the splash-up at time instant $t(g/H)^{1/2} = 9.35$.

B. Two-phase solution

In this section we study the same case by using a two-phase SPH model. The maximum spatial resolution used in this case is $H/\Delta x = 400$ which corresponds to 320,000 water particles and 2,258,000 air particles. For this resolution, using the inequality (25), the time step is $\Delta t \simeq 10\mu s$ and, since the final time is $t = 2.5$ seconds, the number of iterations required is about 250,000.

This simulation has run for 2 days on a cluster machine using 200 cores (Intel Xeon 5500 2.8 GHz). For a 3D simulation with the same spatial resolution around 2.5 billions of nodes would be needed (the same order of node number as used in 38) which, together with the small time step

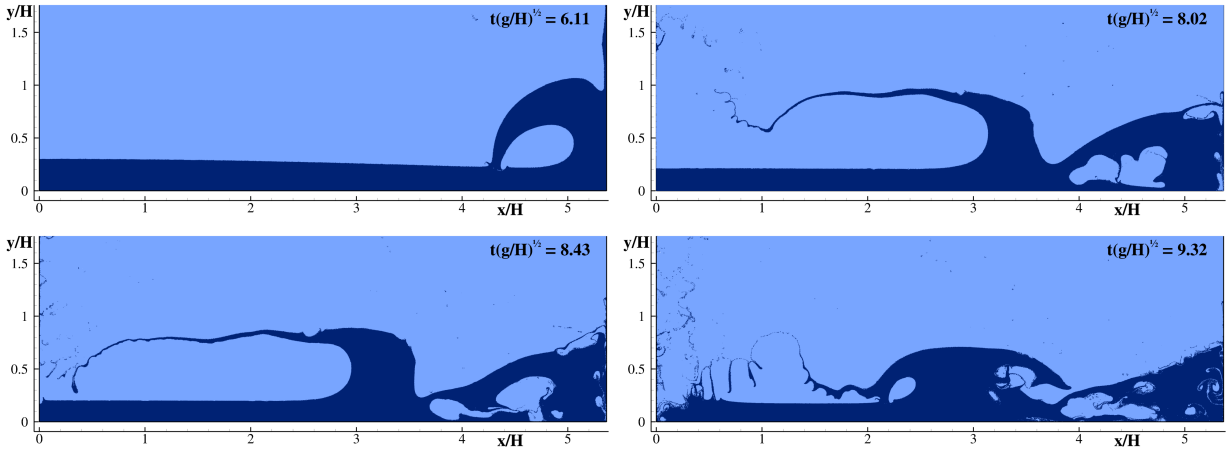

FIG. 7: Confined dam-break flow: SPH time evolution of the two-phase simulation. The plots refer to time instants $t\sqrt{g/H} = 6.11, 8.02, 8.43, 9.35$. (Two-phase model).

required to model the air phase, would make it, even nowadays, quite challenging and is therefore postponed to future works.

Consistently with the previous section, the Reynolds number for the water, $\mathrm{Re}_{water} = H\sqrt{Hg}/\nu_{water}$, has been fixed to 5000 and the physical ratios:

$$\frac{\rho_{air}}{\rho_{water}} = 10^{-3}\,, \qquad \frac{\nu_{air}}{\nu_{water}} = 10$$

are used (see table I). Figure 7 shows four snapshots of the air-water domains during the time evolution. Until time $t(g/H)^{1/2} = 6.1$ the air-water interface is virtually the same as the one obtained with the single-phase model: the role of the air phase is thus negligible, also in terms of dissipation. Next, at the cavity closure, the pressure field his affected by the air-cushioning effect, as documented in Colagrossi and Landrini [7]. Further, during the splash-up stage, the air-water evolution is quite different with respect to the one calculated with the single-phase model, as expected. The closure of the cavity follows a different evolution, and complex drop/bubble dynamics can be recognised. The height of the upwelling water column is lower than the one formed with the single-phase model. However, the fast thin jet, released during the splash-up, contains more mass, momentum and mechanical energy with respect to the single-phase case; in particular, about 20% of the initial water mechanical energy is stored in this jet. This jet is fragmented into several drops during its free fall, causing a large dissipation in the air phase induced by the cloud of drops. Besides the above differences between the evolutions of the single-phase and two-phase cases, the mushroom-like structure, generated by the collapsing of

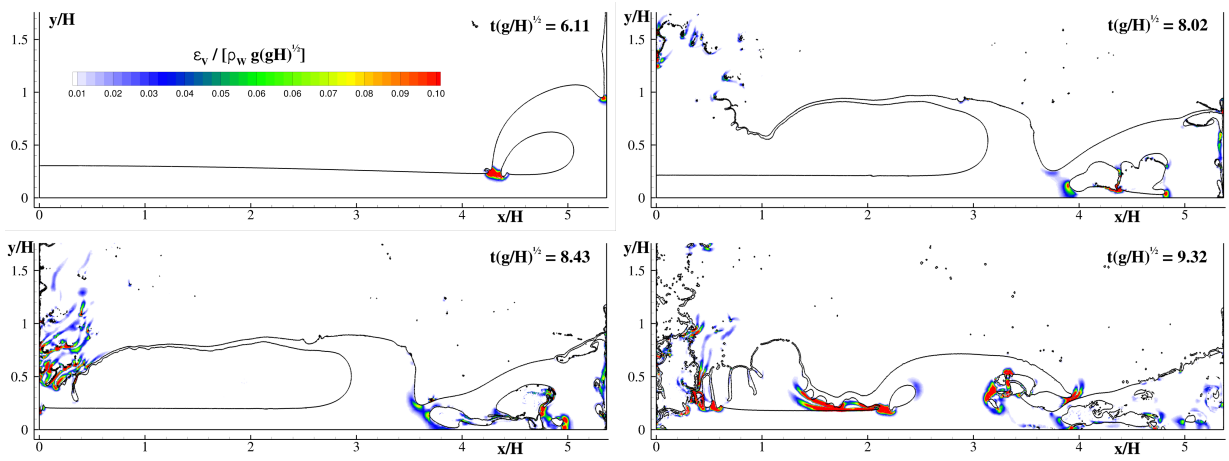

FIG. 8: Contour of the volume-specific dissipation ϵ_V (see eq. 15) for four time instants using a spatial resolution $H/\Delta x = 400$. (Two-phase model).

the upwelling water column, is still present in both simulations.

Figure 8 shows for the same time instants as of section V A the specific energy dissipation field, in both air and water. From the last two frames, it is possible to see that non-negligible viscous dissipation occurs in air. This can be read as a counter-intuitive result; however, even if the viscous ratio $\mu_{air}/\mu_{water} = 0.01$ is quite small, the velocity gradients in the air are much higher (about ten times more than the velocity gradients in water). In fact, especially during impact stages, the air is energetically pushed by the collapse of the water fronts. Furthermore, boundary layers are also formed in air around the falling water drops. As a consequence the two power terms $\mathcal{P}_{V\,water}$ and $\mathcal{P}_{V\,air}$ are of the same order of magnitude.

As a consequence the viscous dissipations $\mathcal{Q}_{V\,water}$ and $\mathcal{Q}_{V\,air}$ are comparable as shown in figure 9. This result is consistent with what was found by Iafrati et al. [20] where a deep-water breaking wave dynamics was studied. Specifically, for the case studied in this section, the viscous dissipation in the water phase is dominant up to $t\sqrt{g/H} < 9$, while at the end of the simulation the viscous dissipation in the air phase becomes larger than in the water. This is mainly due to the fragmentation of the splash-up jet with the consequent formation of several small water drops. The latter dissipate their mechanical energy because of the air drag action. Note that surface tension effects, neglected here, shall be further investigated in this part of the flow.

In figure 10 the time evolution of the mechanical energy decay for the water phase is plotted and compared with the one obtained with the single-phase model. As commented in section III B, $\mathcal{E}_{M\,water}$ decreases almost monotonically, but in a smoother way here. Actually, conversely to

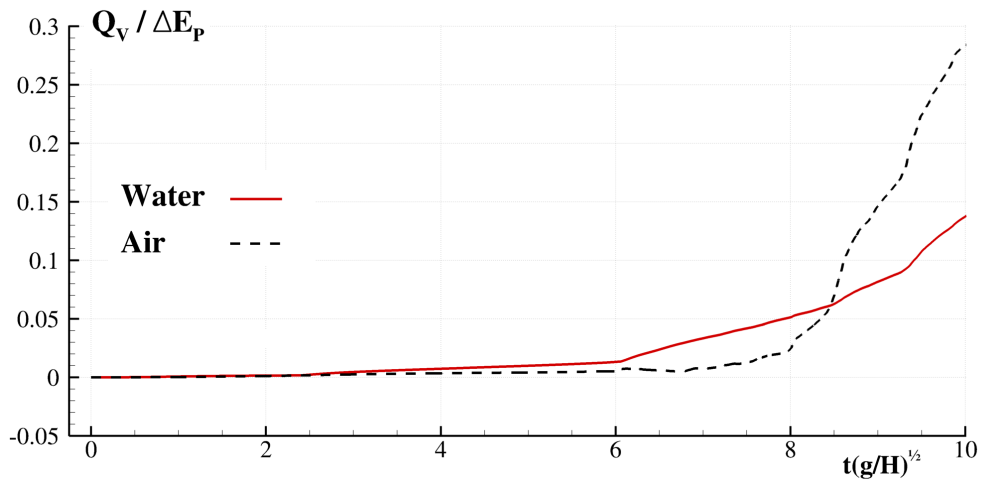

FIG. 9: Comparison of the SPH viscous dissipation terms $Q_{V\,water}$ and $Q_{V\,air}$ during the confined dam-break flow evolution. (Two-phase model).

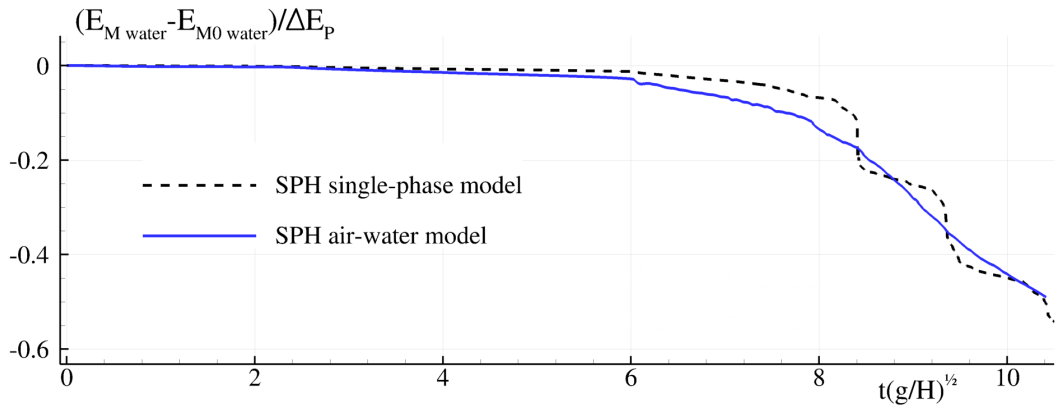

FIG. 10: Comparison of the mechanical energy decay between SPH single-phase (dashed) and SPH two-phase model (solid) during the confined dam-break flow evolution. (Two-phase model).

the single-phase model, there are no energy jumps connected with the empty cavity collapses. Remarkably, besides the many differences between the single-phase and the two-phase solutions, the mechanical energies dissipated during this complex breaking flow evolution are not so different. At time $t(g/H)^{1/2} = 10$, both the models predict an energy decay of 45%. This result, if confirmed in more general cases, may justify the use of single-phase approximation for simulating complex free-surface flows also when air trapping is not negligible. Note again that this kind of single-phase simulation of complex free-surface problems involving breaking waves is common practice by SPH users.

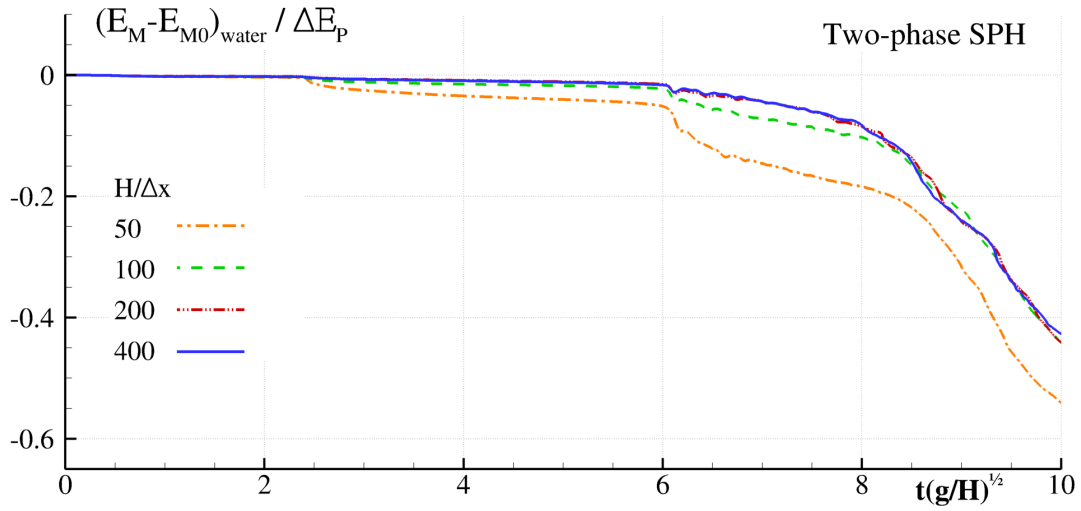

FIG. 11: Time histories of the SPH mechanical energy of the water phase varying the spatial resolution. (Two-phase model).

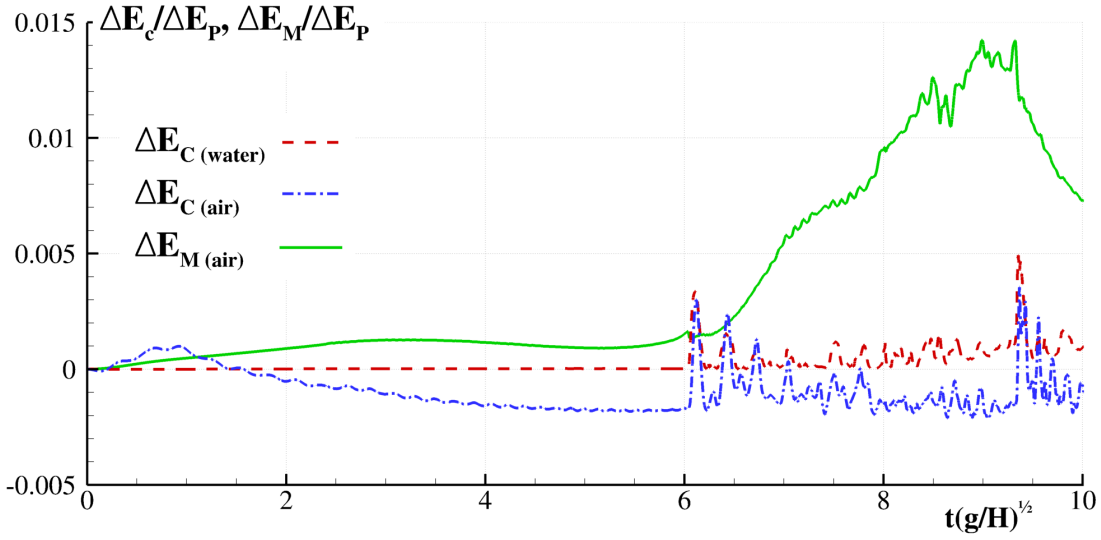

FIG. 12: Time histories of the SPH energy terms $\Delta\mathcal{E}_{C\,water}$, $\Delta\mathcal{E}_{C\,air}$ and $\Delta\mathcal{E}_{M\,air}$. (Two-phase model).

Figure 11 depicts the time evolution of the mechanical energy decay for the water phase predicted by the two-phase SPH solver with varying the spatial resolution. This plot shows that global convergence of the SPH results is attained. Small local differences can be related to the water drops formation and evolution which, in absence of surface tension modelling, is limited only by the spatial discretisation.

Finally, in figure 12 time histories of the energy terms $\Delta\mathcal{E}_{C\,water}$, $\Delta\mathcal{E}_{C\,air}$ and $\Delta\mathcal{E}_{M\,air}$ are

reported. Those components are practically negligible with respect to the others, thus confirming the hypotheses discussed in section III B.

VI. CONCLUSIONS

In the present work the assessment of single-phase approximation to model complex free-surface flows has been investigated. The analysis has been performed on the base of energy considerations, using both single-phase (water only) and two-phase (air-water) models.

The Smoothed Particle Hydrodynamics solver was adopted as investigation tool. This solver was chosen because of its conservation properties (mass, momenta and energy) and because of its ability to accurately describe the interface evolution also during its large deformation and fragmentation.

In order to get convergent results quite high spatial resolutions have been considered. This constraint limits the analysis to ad-hoc 2D test cases. The test case selected is a dam-break flow in a confined domain. Actually, this test case involves a complex flow evolution including the formation of a large shallow water breaking wave followed by multiple splash-up events.

For the single-phase model a cross-validation was performed with a Finite Volume Level-Set approach. The results proved that the energy dissipation evaluated with a weakly-compressible particle method and that one calculated with an incompressible mesh-based solver are quite close. The same test case is then solved using an air-water SPH model, where the air phase is modelled as a compressible gas considering realistic values of the Euler number. This choice implies very small time steps and high computational costs even in a 2D framework.

With respect to the single-phase model, the main results obtained with the two-phase model are:

i) after a similar initial stage up to when the plunging breaker touches the interface, the flow evolution becomes quite different during the splash-up phase, as expected;

ii) the mechanical energy dissipation process is smoother in time and not related to specific flow features such as the cavity collapses or the jet impacts;

iii) beside these differences, the amount of mechanical energy dissipated remains close to the one evaluated with the single-phase model.

The last item is in agreement with the previous works [9], [10], [11]. In these articles it is shown that even using a single-phase model the viscous dissipation is correctly evaluated. The present contribution confirms those results and inspects the mechanisms behind these behaviours, that is, the energy dissipation mainly occurs in impacts and cavity collapses in the single-phase model while, in the two-phase model, it is mainly due to the viscous dissipation at the air-water interfaces.

The present and the above mentioned works consider only shallow water flows in a confined domain. In order to identify a general criterion for the appropriateness of the single-phase approximation the present investigation has to be extended to other flow regimes, as for example breaking waves in deep water condition as the ones we have in ocean.

Finally, the last result we found is that using the two-phase model, at least for the Reynolds regime considered, the viscous heating in air and in water is of the same order of magnitude. This counter-intuitive result has been confirmed also by the recent literature for deep-water breaking wave [20].

VII. ACKNOWLEDGEMENTS

The present work started during the post-doc of Dr. Marrone at the Ecole Centrale de Nantes (ECN) under the supervision of Prof. David Le Touzé. The work was supported later by the CNR-INSEAN Project ENSiS: ENhanced Sph Schemes for complex free-surface flows, funded by the Ecole Centrale de Nantes (ECN).

The SPH simulations performed in the frame of the present research have been obtained by the SPH-Flow solver, a software developed in the framework of a collaborative consortium composed of Ecole Centrale de Nantes, NextFlow Software company and CNR-INSEAN.

The research activity was also partially supported by the Flagship Project RITMARE - Italian Research for the Sea - coordinated by Italian National Research Council and funded by Italian Ministry of Education, University and Research within Nat. Res. Program 2015-2016.

---

[1] J. Rogers and W. Szymczak, Phil. Trans. R. Soc. Lond. A **355**, 649 (1997).

[2] S. Marrone, A. Colagrossi, A. Di Mascio, and D. Le Touzé, Journal of Fluids and Structures **54**, 802 (2015).

[3] A. Colagrossi, B. Bouscasse, and S. Marrone, Phys. Rev. E **92**, 053003 (2015).

[4] H. G. Hornung, C. Willert, and S. Turner, Journal of Fluid Mechanics **287**, 299 (1995).

[5] M. Antuono, A. Colagrossi, D. Le Touzé, and J. J. Monaghan, International Journal for Numerical Methods in Fluids **72**, 583 (2013), ISSN 1097-0363.

[6] M. Landrini, A. Colagrossi, M. Greco, and M. Tulin, Ocean Engineering **53**, 111 (2012), ISSN 0029-8018.

[7] A. Colagrossi and M. Landrini, J. Comp. Phys. **191**, 448 (2003).

[8] R. Bagnold, Journ. of ICE **12**, 202 (1939).

[9] M. Landrini, A. Colagrossi, M. Greco, and M. P. Tulin, Journal of Fluid Mechanics **591**, 183 (2007).

[10] B. Bouscasse, A. Colagrossi, A. Souto-Iglesias, and J. L. Cercos-Pita, Physics of Fluids (1994-present) **26**, 033103 (2014).

[11] B. Bouscasse, A. Colagrossi, A. Souto-Iglesias, and J. L. Cercos-Pita, Physics of Fluids (1994-present) **26**, 033104 (2014).

[12] A. Colagrossi, A. Souto-Iglesias, M. Antuono, and S. Marrone, Phys. Rev. E **87**, 023302 (2013).

[13] P. Madsen and H. Schaffer, Coastal Engineering **53**, 93 (2006), ISSN 0378-3839.

[14] Z. Zapryanov and S. Tabakova, *Dynamics of bubbles, drops and rigid particles*, vol. 50 (Springer Science & Business Media, 2013).

[15] S. Zhang, D. K. Yue, and K. Tanizawa, Journal of Fluid Mechanics **327**, 221 (1996).

[16] A. Korobkin, Journal of Fluid Mechanics **307**, 63 (1996).

[17] M. Cooker, Journal of Engineering Mathematics **44**, 259 (2002), ISSN 0022-0833.

[18] J. H. Seo and Y. J. Moon, Journal of Computational Physics **218**, 702 (2006).

[19] P. Lubin, S. Vincent, S. Abadie, and J.-P. Caltagirone, Coastal Engineering **53**, 631 (2006), ISSN 0378-3839.

[20] A. Iafrati, A. Babanin, and M. Onorato, Phys. Rev. Lett. **110**, 184504 (2013).

[21] J. Monaghan and R. A. Gingold, Journal of Computational Physics **52**, 374 (1983).

[22] J. J. Monaghan, Reports on Progress in Physics **68**, 1703 (2005).

[23] A. Colagrossi, M. Antuono, A. Souto-Iglesias, and D. Le Touzé, Physical Review E **84**, 026705 (2011).

[24] A. Colagrossi, M. Antuono, and D. Le Touzé, Physical Review E **79**, 056701 (pages 13) (2009).

[25] N. Grenier, M. Antuono, A. Colagrossi, D. L. Touzé, and B. Alessandrini, Journal of Computational Physics **228**, 8380 (2009), ISSN 0021-9991.

[26] N. Grenier, D. L. Touzé, A. Colagrossi, M. Antuono, and G. Colicchio, Ocean Engineering **69**, 88 (2013).

[27] J. P. Morris, P. J. Fox, and Y. Zhu, Journal of Computational Physics **136**, 214 (1997).

[28] D. Molteni and A. Colagrossi, Computer Physics Communications **180**, 861 (2009).

[29] A. Ferrari, M. Dumbser, E. F. Toro, and A. Armanini, Computers & Fluids **38**, 1203 (2009), ISSN 0045-7930.

[30] M. Antuono, A. Colagrossi, S. Marrone, and D. Molteni, Computer Physics Communications **181**, 532 (2010), ISSN 0010-4655.

[31] M. Antuono, S. Marrone, A. Colagrossi, and B. Bouscasse, Computer Methods in Applied Mechanics and Engineering **289** (2015).

[32] G. Colicchio, A. Colagrossi, M. Greco, and M. Landrini, Shiffstechnik (Ship Technology Research) **49**, 95 (2002).

[33] S. Marrone, M. Antuono, A. Colagrossi, G. Colicchio, D. Le Touzé, and G. Graziani, Computer Methods in Applied Mechanics and Engineering **200**, 1526 (2011), ISSN 0045-7825.

[34] M. Antuono, A. Colagrossi, and S. Marrone, Computer Physics Communications **183**, 2570 (2012).

[35] L. Lobovský, E. Botia-Vera, F. Castellana, J. Mas-Soler, and A. Souto-Iglesias, Journal of Fluids and Structures **48**, 407 (2014), ISSN 0889-9746.

[36] A. Iafrati, Journal of Fluid Mechanics **622**, 371 (2009).

[37] P. Bonmarin, J. Fluid Mech. **209**, 405 (1989).

[38] P. Lubin and S. Glockner, Journal of Fluid Mechanics **767**, 364 (2015).